



TITLE:

Lymph nodes harbor viral reservoirs that cause rebound of plasma viremia in SIV-infected macaques upon cessation of combined antiretroviral therapy.

AUTHOR(S):

Horiike, Mariko; Iwami, Shingo; Kodama, Makoto; Sato, Akihiko; Watanabe, Yuji; Yasui, Mika; Ishida, Yuki; Kobayashi, Takeshi; Miura, Tomoyuki; Igarashi, Tatsuhiko

CITATION:

Horiike, Mariko ...[et al]. Lymph nodes harbor viral reservoirs that cause rebound of plasma viremia in SIV-infected macaques upon cessation of combined antiretroviral therapy.. *Virology* 2012, 423(2): 107-118

ISSUE DATE:

2012-02-20

URL:

<http://hdl.handle.net/2433/153287>

RIGHT:

© 2011 Elsevier B.V.; This is not the published version. Please cite only the published version.; この論文は出版社版ではありません。引用の際には出版社版をご確認ご利用ください。

Lymph nodes harbor viral reservoirs that cause rebound of plasma viremia in SIV-infected macaques upon cessation of combined antiretroviral therapy

Mariko Horiike¹, Shingo Iwami^{1, 2, 3}, Makoto Kodama⁴, Akihiko Sato⁴, Yuji Watanabe¹, Mika Yasui¹, Yuki Ishida¹, Takeshi Kobayashi¹, Tomoyuki Miura¹ and Tatsuhiko Igarashi^{1#}

¹Laboratory of Primate Model, Experimental Research Center for Infectious Diseases, Institute for Virus Research, Kyoto University, Kyoto 606-8507, Japan, ²Precursory Research for Embryonic Science and Technology (PRESTO), Japan Science and Technology Agency (JST), Kawaguchi, Saitama 332-0012, Japan, ³Graduate School of Mathematical Sciences, The University of Tokyo, Meguro-ku, Tokyo 153-8914, Japan, and ⁴Medical Research Laboratories, Shionogi & Co. Ltd., Osaka 566-0022, Japan.

[#]Corresponding author:
Room 301
Molecular Biology Research Bldg
Institute for Virus Research
Kyoto University
53 Kawahara-cho, Shogoin,
Sakyo ward
Kyoto, Kyoto 606-8507, Japan
+81 75-751-3982 (Ph)
+81 75-761-9335 (Fax)
tigarash@virus.kyoto-u.ac.jp (e-mail)

ABSTRACT

Attempts to find a cure for HIV infection are hindered by the presence of viral reservoirs that resist highly active antiretroviral therapy. To identify the properties of these reservoirs, four SIV239-infected Rhesus macaques were treated with combined antiretroviral therapy (cART) for 1 year. While plasma viral RNA (vRNA) was effectively suppressed, a systemic analysis revealed that vRNA was distributed in the following order: lymphatic tissues > lungs and intestine > other tissues. Histochemistry yielded no cells with viral signals. To increase the chance of detection, two additional SIV-infected animals were treated and analyzed on Day 10 after the cessation of cART. These animals exhibited similar vRNA distribution patterns to the former animals, and immunohistochemistry revealed Nef-positive T lymphocytes predominantly in the follicles of mesenteric lymph nodes (MLNs). These data suggest that lymphatic tissues, including MLNs, contain major cellular reservoirs that cause rebound of plasma viremia upon cessation of therapy.

KEYWORDS

SIV, antiretroviral therapy, HIV-1, HAART, rebound of plasma viremia, reservoirs, animal model.

INTRODUCTION

Highly active antiretroviral therapy (HAART), which consists of three or more anti-HIV-1 drugs, is currently the primary choice of therapeutic intervention for HIV-1-infected individuals (<http://aidsinfo.nih.gov/contentfiles/AdultandAdolescentGL.pdf>). The circulating viral loads in these patients are, in most cases, effectively suppressed below the limit of detection (<50 copies/ml of plasma) by HAART (Richman, 2001). However, the virus loads promptly rebound to pretreatment levels upon cessation of HAART (Chun et al., 1999), which suggests the persistence of viral reservoirs during the combined antiviral therapy. Therefore, to achieve a complete cure of HIV-1 infection, it is essential to eradicate these viral reservoirs.

Resting CD4⁺ T lymphocytes have been identified as a viral reservoir (Chun et al., 1997; Finzi et al., 1997; Wong et al., 1997). These cells harbor intact viral genomes integrated into their chromosomes and produce infectious virus particles when they are reactivated in response to stimulation. It is noteworthy that the estimated half-life of a resting CD4⁺ T cell is more than 44 months (Siliciano et al., 2003), which provides a theoretical basis for the source of the virus that rebounds upon cessation of long-term, successful HAART. Resting CD4⁺ T lymphocyte are probably not the only reservoir of HIV-1. In the majority of patients on HAART, the rebounding viral genotypes detected in the plasma upon cessation of therapy were dissimilar to the genotypes extracted from resting CD4⁺ T cells or from virus particles recovered from cells that were collected before interruption of the therapy (Chun et al., 2000).

Follicular dendritic cells (FDCs) have also been proposed as a viral reservoir (Spiegel et al., 1992). These cells are present in the follicles formed in all secondary lymphoid tissue. Rather than being infected with virus, FDCs retain infectious HIV-1 particles on the cell surface and transfer them to CD4⁺ T lymphocytes (Burton et al., 2002). Since FDCs retain numerous virus particles, the genomes of which exhibit greater diversity than those in other tissues or cells and which reportedly hold infectious particles for months to years, it seems likely that these cells serve as archives of infectious virions (Keele et al., 2008).

The recently developed method for ultrasensitive detection of plasma viral

burdens has revealed that patients who have HAART-controlled viremia (below the detection limit by clinical criteria; i.e., <50 copies/ml plasma) over several years still harbor minuscule amounts of virion-associated RNA in the circulation (Palmer et al., 2008), suggesting ongoing viral replication, i.e., “residual viremia”. The potential for ongoing HIV-1 replication during HAART is supported by evidence of *env* gene evolution in patients receiving HAART (Frost et al., 2001; Martinez et al., 1999), as well as the detection in patients on HAART of 1-LTR and 2-LTR circles, episomal HIV-1 cDNAs, the presence of which most likely reflects recent infection (Sharkey et al., 2005; Sharkey et al., 2000). A transient increase in the number of 2-LTR circles, probably reflecting an increase in the number of failed attempts to integrate into the host cell genome, was detected in approximately 30% of infected individuals who were receiving HAART, when an integrase inhibitor was added as treatment intensification (Buzon et al., 2010). Based on these lines of evidence, it is conceivable that certain cell types, as yet to be identified, allow productive replication of HIV-1 during HAART. Although HAART theoretically arrests *de novo* virus replication, these unidentified reservoirs appear to be refractory to the antiviral effects of the regimen through unknown mechanisms.

It is postulated that viral reservoirs in the host retain HIV-1 during HAART as follows: resting CD4⁺ T lymphocytes store inducible viral genomes, FDCs archive infectious particles, and unidentified cells support productive viral replication cycles. It remains to be revealed whether other cell types serve as viral reservoirs using other mechanisms, and which cell type is the most important for sequestering HIV-1.

Peripheral blood samples from volunteer patients have been used in studies to identify HIV-1 reservoirs (Brennan et al., 2009; Chun et al., 2000; Sharkey et al., 2011). However, HIV-1 predominantly replicates in CD4⁺ T lymphocytes in the lymphoid tissues (Embretson et al., 1993; Pantaleo et al., 1993), particularly the intestine, which is home to 70-90% of all lymphocytes in the body and which is severely affected during the acute phase of infection (Brenchley et al., 2004; Guadalupe et al., 2003), determining prognosis. Therefore a systemic analysis, in addition to existing studies on peripheral blood, would elucidate the mechanisms underlying rebound of plasma viremia upon discontinuation of HAART. Since it is unethical to collect various tissues from patients for analysis, an alternative model system is required. In this regard, the SIV/macaque model, which has been useful in understanding HIV-1 infection, is

1 suitable for investigations of viral reservoirs using a systemic analysis (Dinoso et al.,
2 2009; North et al., 2009).

3 Using the SIV239/monkey system, we investigated HIV-1 reservoirs during
4 combined antiretroviral therapy (cART). First, we conducted a systemic analysis of
5 SIV-infected Rhesus monkeys that received cART for an extended period. SIV239 has
6 been extensively used as a tractable animal model for HIV-1 in studies of replication,
7 pathogenesis, and vaccine development. In addition, this virus causes almost complete
8 depletion of CD4⁺ T lymphocytes in the intestine (Veazey et al., 1998), as HIV-1 does in
9 patients who suffer from AIDS.

RESULTS

Establishment of anti-SIV239 cART regimen with oral administration

Before the experimental infection of macaques with SIV, we established an antiretroviral regimen that is applicable to SIV239 infection in the Rhesus macaque model. Given that NNRTIs do not suppress replication of SIV (Balzarini et al., 1995), anti-HIV-1 drugs belonging to this class were excluded from consideration. Regarding NRTIs, several studies have confirmed that Tenofovir (TDF) and its pro-drug PMPA are effective against SIV. Some studies have used Zidovudine (AZT) and Lamivudine (3TC) to suppress SIV replication *in vitro* and *in vivo* (Balzarini et al., 1995; Benlhassan-Chahour et al., 2003). Based on the results of these studies, we included TDF (Viread) and AZT/3TC (Combivir) in our regimen. Regarding protease inhibitors (PIs), Saquinavir (SQV) has been shown to be effective against SIV *in vitro* (Giuffre et al., 2003; Witvrouw et al., 2004). When we initiated this study, the anti-SIV efficacies of other commercially available PIs had not yet been reported. To determine which PI to include in our cART, we examined three commercially available PIs—SQV, Lopinavir/Ritonavir (LPV/RTV; Kaletra), and Atazanavir (ATV; Reyataz)—in the MT-4/MTT assay. This assay, which was originally developed to measure cell proliferation, was used to evaluate inhibition of virus-induced killing of human T-lymphoid MT-4 cells in the presence of increasing amounts of the drugs (Pauwels et al., 1988). Along with SIV239, HIV-1 IIIB was employed in the assay as a control. All of the compounds tested suppressed the activity of SIV239. The EC₅₀ values for SQV were 18.5 nM against SIV and 22.7 nM against HIV-1 (Table 1 and Supplemental Figure 1). The EC₅₀ ratio, i.e., the EC₅₀ value against SIV divided by the EC₅₀ value against HIV-1, was 0.8 (Table 1). The EC₅₀s against SIV239 and the EC₅₀ ratios of the other two drugs were: 52.2 nM and 1.5, respectively, for LPV/RTV; and 80.0 nM and 4.7, respectively, for ATV. Pharmacokinetic information on these drugs is available, and the half-life in the circulation in humans is: 1–2 h for SQV; 5–6 h for LPV/RTV; and 7 h for ATV (<http://aidsinfo.nih.gov/contentfiles/AdultandAdolescentGL.pdf>). Taking into account the EC₅₀, the half-life (which defines the required frequency of administration to maintain the drug level), and cost-effectiveness, we included LPV/RTV in our regimen.

Drug administration was instituted *per os*, to effectively model the metabolism and pharmacokinetics of the antiviral drugs in patients. The dosage and

administration of these drugs are described in the *Materials and Methods* section. To assess whether a given dosage resulted in a measurable concentration of the drug in the circulation even after a long interval, blood samples were collected from six monkeys at 14 h after intake and the antiviral effect in plasma was determined by titration. The drug concentrations in the animals' blood ranged from 7.2–29.5 μM (LPV/RTV equivalent); these levels are 5- to 20-fold higher than those recommended for adult patients (1.5 μM for LPV/RTV equivalent) (<http://aidsinfo.nih.gov/contentfiles/AdultandAdolescentGL.pdf>). Plasma samples from two representative animals, which had already been measured in the biological assay, were also subjected to HPLC. The results of the HPLC analysis revealed drug concentrations comparable to those determined by the biological assay: 16.1 μM for one animal (20.0 μM by the MTT assay) and 25.7 μM for the other animal (24.8 μM by the MTT assay), thus justifying our use of the biological assay to measure levels of antiviral activity in the circulation of SIV-infected animals during therapy. Based on these results, we finalized the regimen.

Efficacy of the cART regimen for macaques infected with SIV239

The establishment of the anti-SIV regimen enabled us to conduct animal experiments. Seven Rhesus macaques were inoculated intravenously with 2,000 TCID₅₀ of the SIV239 virus stock. All animals exhibited an initial peak of viremia at 2 weeks post-inoculation (pi) (median, 2.2×10^7 copies/ml; range, $7.9\text{--}60.0 \times 10^6$ copies/ml, Figure 1). At 8 weeks pi, when the viral loads decreased from the initial peak and plateaued (median, 1.3×10^5 copies/ml; range, $1.1\text{--}4.9 \times 10^5$ copies/ml), the cART was administered to four of the monkeys (MM491, MM499, MM528, and MM530; designated as group A).

Upon drug administration, the plasma viral RNA (vRNA) levels in these animals promptly started to decrease. There was an inverse inclination between set point plasma vRNA load and duration to suppress vRNA to the detection limit (200 copies/ml). The vRNA of MM491, whose set point viral RNA level was the lowest in the group 1.1×10^5 copies/ml, fell below the detection limit in 2 weeks. MM499 and MM528, whose plasma vRNAs were 4.4×10^5 and 1.3×10^6 copies/ml at the initiation of cART, took 5 and 6 weeks, respectively. After nine weeks of treatment, the viral burden of MM530, which had the highest level in the group at 4.9×10^6 copies/ml, was undetectable. Plasma

vRNA levels of all animals on cART had fallen below the limit of detection by 17 weeks pi. When HAART was applied to SIV/pigtailed macaque or RT-SHIV/rhesus macaque models, it took 8 and 18 weeks, respectively, to suppress circulating vRNA to below the detection limit (Dinoso et al., 2009; North et al., 2009). When considering variables from previous studies, including virus strain, drug combinations, detection limit of vRNA measurement, and initiation of treatment of these studies, it is conceivable that the cART approach devised in the current study is as potent in terms of the progress to viral containment.

To relate our results to previous studies on vRNA declines for HIV-1 and SIV following antiviral therapy, we examined the levels of viremia in our infected monkeys during the first few weeks after the initiation of therapy (Table 2 and Supplemental Figure 2). Each individual monkey followed a similar pattern of viral decay: an initial rapid and exponential reduction by almost 2.5 orders of magnitude (comprising the first phase, which is presumably associated with short-lived infected cells), followed by a slower exponential decline of 1.5 orders of magnitude (the second phase, which is presumably associated with long-lived infected cells). The observed biphasic decay of viral burdens was consistent with previous findings from studies on SIV models and patients with HIV-1 (Dinoso et al., 2009; Murray et al., 2007; Perelson et al., 1997; Perelson and Nelson, 1999). Decay rates for the first and second phases were deduced by employing mathematical modeling (Table 2). The decay rates of the first phase ranged from 0.495 (for MM491) to 0.853 (for MM499), and those of the second phase ranged from 0.028 (for MM491) to 0.089 (for MM499). The decay rates of plasma vRNA loads during the first phase in patients with HIV-1 on HAART, consisting of LPV/RTV, Efavirenz, 3TC, and TDF, exhibited comparable numbers to those in the current study, ranging from 0.6 to 1.4 (Markowitz et al., 2003). Mean half-lives of ($\log_2/a =$) 1.13 for the first phase and ($\log_2/\mu_M =$) 14.24 days for the second phase

were comparable to those observed in patients with HIV-1 on HAART. Half-lives of HIV-1 RNA in the circulation of HIV-1-infected patients on suppressive ART, consisting of Indinavir and Efavirenz, ranged from 0.6 to 2.0 days for the first phase and 5.2 to 35.6 days for the second phase (Havlir et al., 2003). Comparison of the viral decay rates derived in the current study with those derived in previous reports (Perelson et al., 1997) gave statistically insignificant results ($P = 0.667$ for the first phase, and $P = 0.662$

for the second phase). These results suggest that the virologic response of SIV infected Rhesus macaques to cART, as reported in a recent study (Dinosa et al., 2009), is comparable to the response of HIV-1-infected patients to HAART.

Patients with HIV-1 on HAART exhibit undetectable levels of plasma vRNA (typically less than 50 copies/ml) when the therapy works as expected. To estimate suppression levels achieved by the regimen used in the current study, selected plasma samples with adequate volume from animals in group A were subjected to another quantitative real-time PCR assay with a lower detection limit. Using 1.5-ml plasma samples, which were collected at 29, 42, and 52 weeks pi, and at euthanasia, particle-associated vRNA was extracted and amplified. All of these samples yielded less than 20 copies/ml of vRNA loads (Table 3), except for those collected at 42 and 52 weeks pi (44 and 47 copies/ml, respectively) from MM530, which exhibited the highest plasma vRNA at the start of cART (4.9×10^6 copies/ml) and required the longest duration to suppress vRNA to 200 copies/ml (9 weeks). These results confirm that the regimen established in the current study is as suppressive as those applied to patients. Based on the progression to viral containment, decay rates, and suppression levels, we concluded that the cART established in the current study is comparable to therapies used to treat patients with HIV-1 and suitable to pursue viral reservoirs during therapy. The suppressed viral burdens of the treated animals were maintained below the limit of detection throughout the course of treatment (up to 52 weeks). In contrast, the viral burdens of the untreated animals (MM496, MM510, and MM521) remained at $>1.0 \times 10^5$ copies/ml until the day of necropsy (Figure 1). Assuming a limit of viral detection of 200 copies/ml, there was a statistically significant difference in the plasma vRNA levels between the two groups of animals at Week 42 ($P < 0.05$).

During the entire course of cART, the levels of antiviral activity in the plasma samples of animals MM491, MM528, and MM530 assessed by MT-4/MTT assay were above the recommended trough level for adult patients (for MM491: range, 3.5–17.8 μ M LPV/RTV equivalent; for MM528: range, 6.0–24.9 μ M LPV/RTV equivalent; for MM530: range, 8.2–14.2 μ M LPV/RTV equivalent) (Table 4). Even in the remaining animal, MM499, in which the circulating concentration of the activity was below the recommended trough level at the two time-points tested, at 10 weeks pi and at autopsy, during the course of antiviral therapy, the plasma vRNA levels were below the limit of detection. None of the treated animals exhibited a transient surge in vRNA level during

the entire course of the therapy. Certain clinical conditions are known to be side-effects of antiviral drug treatment (<http://aidsinfo.nih.gov/contentfiles/AdultandAdolescentGL.pdf>). Among the drugs employed in the present study, TDF potentially causes renal complications (Van Rompay et al., 2004) and LPV/RTV can induce abnormal lipid metabolism. In general, no significant adverse effects were noted for the drugs employed in the present study. We conclude that the antiretroviral therapy regimen established in the current study is as effective as the combined antiretroviral therapy applied to patients with HIV.

Higher titers of vRNA were detected in the lymphoid tissues of virus-infected animals undergoing antiretroviral therapy

The establishment of an effective antiretroviral therapy regimen for SIV-infected monkeys was a prerequisite for the identification of virus reservoirs during combined antiviral therapy. To this end, we considered two important questions: ‘Is virus replication maintained during the therapy?’, and ‘If active virus replication persists, are there particular anatomic compartments that allow preferential virus replication?’

To answer these questions, we looked for the presence of vRNA in a variety of tissues collected from animals receiving cART over a period of 1 year. Total RNA was extracted from each tissue and subjected to real-time reverse transcription (RT)-PCR. Table 5 summarizes the results of RT-PCR for four animals in group A that were subjected to analysis at the end of the 1-year cART regimen, along with a representative animal that was not given treatment (MM521); all the animals were euthanized at between 61 and 68 weeks pi. In the untreated monkey (MM521), vRNA was detected in all the tissues examined, with the exception of the brainstem. In the lymphoid tissues, higher titers of vRNA (approximately 1.0×10^8 copies/ μ g total RNA) were detected. In the gastrointestinal tract, lungs, and vagina, in which the resident $CD4^+$ T-lymphocyte population consists mainly of $CCR5^+$ memory cells (the preferred target of HIV-1 and SIV) (Douek et al., 2003; Meng et al., 2000; Veazey et al., 2000), the vRNA titers were approximately 1.0×10^6 copies/ μ g of total RNA. Lower levels of vRNA were detected in the non-lymphoid tissues (heart, liver, and kidneys) and the central nervous system (cerebrum and cerebellum).

In the group A macaques, the vRNA titers in several tissues were much lower

than those found in the untreated animals. The non-lymphoid tissues and central nervous system did not contain measurable amounts of vRNA. Low levels of vRNA were detected in the effector sites, such as the intestine (up to 6.5×10^4 copies/ μ g total RNA), lungs, and vagina (up to 6.5×10^3 copies/ μ g total RNA). Statistical analysis of vRNA burdens revealed significant reductions in the jejunum and rectum of animals in group A as compared to those of untreated controls ($p = 0.03$), indicating that cART suppressed vRNA expression in those tissues, although incompletely. Compared to the above-mentioned tissues, higher levels of vRNA (approximately 1.0×10^5 copies/ μ g of total RNA) were detected in the lymphoid tissues. Of note, both the superior and inferior mesenteric lymph nodes (sMLNs and iMLNs, respectively) were among the tissues that contained the highest titers of vRNA in animals on cART. Statistical analysis of vRNA in the lymphatic tissues also revealed significant suppression in group A as compared to controls (iliac and submandibular lymph nodes and iMLNs, $p = 0.03$).

To identify the cell type(s) that support vRNA synthesis and, potentially, allow viral proteins to be produced during ART, we prepared tissue sections from the animals in group A and subjected them to *in situ* hybridization (ISH) and immunohistochemistry (IHC). While these tissues yielded no positive signals, the same staining techniques detected vRNA-positive cells and viral-protein-positive cells in tissue sections prepared from untreated animals (data not shown).

In summary, our initial questions were resolved as follows: the presence of vRNA in the gut, lungs, vagina, and lymphoid tissues indicated active viral replication in animals that were treated with cART for 1 year, and the lymphatic tissues allowed preferential viral replication in these animals.

SIV Nef-producing T lymphocytes predominated in the follicles of the MLNs from an animal that exhibited rebound of plasma viremia upon cessation of cART

Quantitative PCR analysis of vRNA in a variety of tissues collected from SIV-infected animals that were on prolonged chemotherapy (i.e., the animals in group A) indicated that the lymphatic tissues acted as the anatomic compartment for active

virus replication during antiretroviral therapy. However, we were unable to identify histochemically any vRNA-positive or viral-protein-positive cells in the tissue sections prepared from these animals. This discrepancy was likely due to the lower sensitivity of these staining techniques as compared to PCR. We assumed that cessation of ART would result in rebound of plasma viremia, thereby promoting the transcription and translation of viral genes to levels detectable by the histochemical staining techniques employed in the present study. Based on this assumption, we took advantage of the rebound of plasma viremia as a surrogate approach to identify the viral reservoir(s) during cART. Thus, two Rhesus macaques (MM508 and MM511, designated as group B animals) were inoculated with the same SIV239 virus stock as was used to inoculate the group A animals. The group B animals exhibited an initial peak of viremia at 2 weeks pi (range, $7.7\text{--}8.4 \times 10^7$ copies/ml; Table 6), and the viral loads decreased and stabilized from 8 wpi onwards. Upon initiation of cART at 38 wpi, the levels of virus decreased rapidly and eventually fell below the limit of detection. The suppressed viral burdens were maintained until cessation of the treatment at 46 weeks pi. We attempted to determine the time-point at which the levels of viral gene transcription and translation were just above the detection limit of our staining. Since we envisioned that rebound of plasma viremia would take place within 2 weeks of interruption of therapy, animals were euthanized for necropsy on Day 10 after cessation of cART. The viral load in the plasma of animal MM511 was 1400 copies/ml, while that of animal MM508 was below the limit of detection (Table 6). Thus, one animal was exhibiting rebound of plasma viremia while the other animal had not yet reached that stage when they were killed for analysis.

The overall tendency of the vRNA distribution in the group B animals was similar to that observed in the group A animals, with the titers being somewhat higher in group B. Higher levels of vRNA ($>1.0 \times 10^4$ copies/ μg total RNA) were detected exclusively in the lymphoid tissues (Table 7). In MM511, the highest level of vRNA was detected in the MLNs ($>1.0 \times 10^6$ copies/ μg total RNA). MM508, in which the plasma viral load was below the limit of detection at euthanasia, contained high levels of vRNA ($>1.0 \times 10^5$ copies/ μg of total RNA), but only in the spleen and iMLN.

Based on the increased levels of vRNA transcription, we hypothesized that higher levels of viral proteins were synthesized in these two animals (MM508 and MM511) than in the group A animals. We subjected all the lymphoid tissues collected

from these two animals to IHC, to identify viral-protein-producing cells. First, we focused on MM511, which exhibited higher viral titers in the plasma and lymphoid tissues than MM508, and stained tissue sections from this animal with anti-Nef antibodies. IHC yielded Nef-positive cells. The viral-protein-positive cells were mainly localized to the globular architecture in the lymph node cortex, most likely the lymphoid follicles, and the Nef-positive cells bore morphologic characteristics similar to those of T lymphocytes (Figure 2a). To clarify the architecture within which the Nef-producing cells were detected, we conducted combined IHC with an anti-Nef antibody (visualized with DAB) and an antibody directed against CD35 (visualized with VECTOR Blue). CD35 is a cell surface marker for FDCs, which are found exclusively in the follicles of the secondary lymphoid tissues. The combined staining showed that Nef-positive cells and FDCs were present in the same globular architecture, suggesting that the viral-protein-producing cells were predominantly located in the follicles of the lymph nodes of this animal. Moreover, staining revealed that the Nef-producing cells were juxtaposed on the FDCs (Figure 2b).

To confirm the identity of the viral-protein-expressing cells, we conducted combined immunofluorescence staining with an anti-Nef antibody (visualized with Alexa Fluor 488) and an anti-CD3 antibody (visualized with Alexa Fluor 594). After extensive observations of the stained sections under the microscope, we detected Nef-positive cells in 16/305 sections prepared from a variety of lymphatic tissues collected from animal MM511, and these viral-protein-expressing cells were all positive for CD3 (Figure 3 and Table 8). Of these 16 sections, 12 were prepared from MLNs and 4 from other anatomical compartments. The viral-protein-producing cells in the follicles constituted around 75% of all the positive cells detected. In some sections, Nef-positive cells were clustered in the follicles (Figure 3c).

In animal MM508, which was subjected to analysis before rebound of plasma viremia had taken place, the staining revealed a single Nef-positive cell that was also positive for CD3 (data not shown). The frequency of positive cells in this animal was substantially lower (one positive cell in 136 sections) than that in MM511.

In summary, in the animal that exhibited rebound of plasma viremia after cessation of cART, almost all the viral-protein-synthesizing cells, presumably productively infected cells, that were detected in the MLNs were identified as T lymphocytes, most likely CD4⁺ T cells. The vast majority of the virus-infected T cells

- 1 were observed in the lymphoid follicles during rebound of plasma viremia (Table 8).
- 2

DISCUSSION

The presence in infected individuals of HIV-1 viral reservoirs that persist during HAART impedes curing and complete eradication of the virus. While studies have been conducted into the identity and properties of the HIV-1 reservoirs (Brennan et al., 2009; Chun et al., 2000; Sharkey et al., 2011), much remains to be learnt. We reasoned that systemic analyses of infected individuals who were undergoing intensive ART would advance the characterization of the viral reservoirs (Dinosa et al., 2009; North et al., 2009). Therefore, we analyzed SIV-infected Rhesus macaques that underwent cART for 1 year. The major finding of the current study is that lymphatic tissues, including MLNs, contained higher numbers of cellular virus reservoirs that potentially cause rebound of plasma viremia upon cessation of cART. This assertion is based on the following observations: the lymphatic tissues contained the highest levels of vRNA in all the animals, regardless of cART, and the viral-protein-expressing T cells were localized predominantly to the MLNs of the animal that exhibited rebound of plasma viremia after cessation of cART.

We finalized the drug dosages to be administered by monitoring plasma trough levels of antiviral activity at 14 h post-consumption. During this process we discovered that the drug metabolism of monkeys is somewhat higher than that of humans. To fine-tune the drug concentrations in the circulation, 50% of the dosage established in the present study, corresponding to 150% of the dosage for a 60-kg adult patient, was given to the same animals. The circulating drug concentration at 14 hours post-consumption yielded no measurable net antiviral activity (data not shown). Therefore, it is necessary to determine an appropriate dosage for each drug prior to administration to animals. In this regard, one of the monkeys in group A, MM499, exhibited fluctuating antiviral activity during the therapy. At 10 and 64 weeks pi, the antiviral activity in the blood were below the recommended trough level for patients (1.5 μ M) (Table 4). Despite the fluctuation of antiviral activity, the viral burden of this animal was maintained below the limit of detection during the therapy, and systemic analysis revealed levels of vRNA that were comparable to those detected in the other three animals in group A (Table 5). That the other three animals also exhibited fluctuating concentrations of the drug in the circulation underlines the importance of monitoring antiviral activity in circulation during therapy, to ensure that the

administration schedule produces the expected antiviral activity.

RT-PCR analyses revealed that lymphatic tissues contained higher titers of vRNA than the other tissues in 4/4 SIV-infected macaques in group A, and 2/2 animals in group B followed the same distribution of vRNA (Table 5 and 7). In SIV-infected monkeys treated with cART, the Lamivudine concentration was more than 300-fold higher in the gastrointestinal tract than in the peripheral lymph nodes (Bourry et al., 2010). The finding of Bourry et al. explains our observation that chemotherapy was more effective at suppressing virus replication in the intestine than in the lymph nodes. It is possible that lymphatic tissues serve as viral sanctuaries, especially when the amount of drug accumulated in the tissues is insufficient to suppress virus replication. It should be noted that while viral load and drug concentration in the plasma are easily monitored, they do not reflect precisely the virus replication/drug distribution in specific important anatomic compartments.

Our results are also in good agreement with the results reported by North et al., who performed a thorough analysis of a variety of tissues collected from RT-SHIV-infected animals that were receiving combined anti-viral therapy (North et al., 2009). The authors employed RT-SHIV, which is a chimeric virus that carries the HIV-1-derived RT gene on the backbone of SIV239, to model HAART to patients, in the context of SIV, since non-nucleotide reverse-transcriptase inhibitors (NNRTIs), one of the core components of HAART, do not suppress reverse transcription mediated by SIV RT (Balzarini et al., 1995). Although the cART regimen devised in the current study is unlike the HAART administered to patients, especially with respect to the employment of certain drugs, the viral decay rate in the circulation (calculated based on a two-compartment model) is comparable to that observed in patients treated with the multi-drug regimen (Murray et al., 2007; Palmer et al., 2008; Perelson et al., 1997) (Table 2 and Supplemental Figure 2). Therefore, it is implied that the lymphatic tissues may harbor higher titers of vRNA in HIV-1-infected patients on HAART, despite the viral burdens in the circulation are clinically non-detectable. The caveat is that the animals in the current study were on treatment for up to 1 year only, which is a considerably shorter treatment period than that of patients who have achieved successful virus containment since the beginning of the HAART era. Given that the desired concentration of the drug may not be reached in the lymphatic tissues, it is necessary to devise a way to deliver in a preferential manner either antiviral drugs or a specific injury

to these compartments, in combination of HAART, to achieve eradication of the virus, which is a crucial step towards a complete cure for HIV-1 infection.

Histochemical analyses revealed that the SIV Nef protein was expressed in T lymphocytes predominantly resident in the follicles formed in the MLNs of animal MM511, which exhibited viral rebound after cessation of cART (Figure 3 and Table 8). Active virus replication in the follicles of lymph nodes has been described (Folkvord et al., 2005). Previous studies have suggested that lymphatic follicles serve as preferred sites of virus replication, probably *via* FDCs and sequestration of virus-infected cells from cytotoxic T lymphocytes (CTLs). FDCs, which may interact with CD4⁺ cells within the “enclave”, retain infectious virus particles and produce TNF- α , which promotes HIV replication (Thacker et al., 2009). HIV-1-specific CTLs fail to accumulate within lymphoid follicles, allowing unchecked virus replication in this architecture (Connick et al., 2007). Taken together, these findings support our observations of active viral protein synthesis in the lymphoid follicles.

The present study does not identify definitively the viral reservoirs. However, it does not rule out any of the proposed candidate reservoirs: resting CD4⁺ T lymphocytes, FDCs, and unidentified cells involved in ongoing virus replication during therapy. To place our results in the context of current thinking regarding putative viral reservoirs, we make the following important points:

North et al. detected proviral DNA in the resting CD4⁺ T-lymphocyte fraction prepared from MLNs (North et al., 2009). Dinoso et al. recovered replication-competent viruses in the cell fraction (Dinoso et al., 2009). It is possible that the Nef-positive cells detected in the current study were reactivated upon stimulation, thereby prompting resumption of the virus replication cycle; the progeny viral particles from these cells would initiate multiple rounds of replication in the T cells of the paracortical area and the follicles of the lymph nodes.

We detected FDCs juxtaposed on the Nef protein-positive T lymphocytes. This observation is not definitive evidence that FDCs transmit infectious viral particles to CD4⁺ T cells. Based on our observations, we hypothesize that FDCs transmit virus to CD4⁺ T cells or stimulate infected cells, so as to initiate viral rebound. An important caveat is that the animal in question was treated for only 8 weeks. Since FDCs are known to retain virus particles with their infectivity intact for a certain period of time (Keele et al., 2008), it would be informative to determine whether the interaction

1 between these two cell types occurs in animals that exhibit rebound after a prolonged
2 period of therapy, followed by cessation.

3 Although we have no direct evidence that unknown cells are involved in
4 ongoing viral replication during therapy, higher titers of vRNA were detected in the
5 lymphatic tissues, primarily the MLNs, which suggests that certain cell types in this
6 compartment allow viral replication during chemotherapy. It is likely that the levels of
7 transcription of viral genes and of subsequent translation are too low to be detected by
8 the staining techniques employed in the current study.

9 Based on our results, we postulate the following sequence of events after the
10 cessation of HAART in individuals infected with HIV-1: in the follicles of the lymph
11 nodes, such as MLNs, viruses that are preserved in certain forms, such as intact
12 genomes and infectious particles, and with low-level ongoing replication, resume a
13 productive replication cycle, preceding other anatomical compartments, when the
14 concentration of the antiviral drug declines due to discontinuation of therapy; thereafter,
15 other anatomic compartments resume productive viral replication owing to weakened
16 containment of the virus and higher accumulations of the drugs. The progeny viral
17 particles produced from the tissues subsequently enter the circulation and cause rebound
18 of plasma viremia, i.e., systemic viral replication.

19 Considering that the state-of-the-art histochemical staining still has lower
20 sensitivity than PCR and that the vRNA distributions for animals on ART and those
21 with rebound of plasma viremia are similar, analyses of animals undergoing rebound of
22 plasma viremia after discontinuation of therapy could serve as a surrogate approach to
23 study virus reservoirs during HAART.

24 Fortunately, we captured ongoing rebound of plasma viremia in animal
25 MM511, whose viral burden was above the detection limit defined by the current
26 staining technique. Further fine-tuning in the duration of therapy and timing of analysis
27 after cessation would provide better clues to the identity of virus reservoirs.

28

MATERIALS AND METHODS

Cells

Human embryonic kidney-derived 293T cells were cultured in Dulbecco's modified Eagle's medium (D-MEM; Invitrogen, Carlsbad, CA) that was supplemented with 10% fetal bovine serum (FBS; HyClone Laboratories, Logan, UT) and 2 mM L-glutamine. Human T-lymphoid MT-4 (Harada et al., 1985), Molt-4 (Koyanagi et al., 1986), and M8166 (Shibata et al., 1991) cells were cultured in RPMI 1640 medium (Invitrogen) that was supplemented with 10% FBS, 2 mM sodium pyruvate, and 4 mM L-glutamine (R-10). Rhesus macaque PBMCs were prepared from whole blood that was anticoagulated with EDTA in lymphocyte separation medium (Nakalai Tesque, Kyoto, Japan). PBMCs were resuspended in R-10 medium that was supplemented with 40 µg/ml gentamicin, 50 µM 2-mercaptoethanol, and 25 µg/ml concanavalin A (Sigma-Aldrich, St. Louis, MO), and cultured for 16–20 h at 37°C. Before virus infection, the cells were cultured for an additional 2 days in R-10 medium that was supplemented with 40 µg/ml gentamicin, 50 µM 2-mercaptoethanol, and 100 IU/ml recombinant human IL-2 (Imunace; Shionogi, Osaka, Japan).

Viruses

The stock of SIV239 used in the tissue culture and animal experiments was prepared in Rhesus macaque PBMCs inoculated with the supernatant of a 293T-cell culture that was transiently transfected with full-length infectious molecular clones of the virus (Kestler et al., 1990). A stock of HIV-1 IIIB (Popovic et al., 1984) was prepared from the supernatant of a Molt-4 cell culture that was chronically infected with the virus. The SIV239 stock was titrated by infection of M8166 cells, and the number of infectious units was calculated by a method described previously (Reed and Muench, 1938).

Animal experiments

Female Rhesus macaques of Chinese or Indian origin, 4 kg in body weight, were used for experimental infection with SIV239. Phlebotomy and virus inoculation were carried out under anesthesia by intramuscular injection of a mixture of ketamine chloride (Ketalar; Daiichi Sankyo, Tokyo, Japan) at 5–10 mg/kg and xylazine chloride (Celactal; Bayer Healthcare, Leverkusen, Germany) at 1.5–2.0 mg/kg. For virus

infection, animals were inoculated intravenously with 2000-times the 50% tissue culture infectious doses (TCID₅₀) of SIV239. Animal experiments were conducted in a biosafety level 3 animal facility, in compliance with institutional regulations approved by the Committee for Experimental Use of Nonhuman Primates of the Institute for Virus Research, Kyoto University, Kyoto, Japan.

Extraction of active components from drug tablets or plasma

Saquinavir (Invirase; Chugai Pharmaceutical, Tokyo, Japan), Lopinavir/Ritonavir (Kaletra; Abbott Laboratories, Abbott Park, IL), and Atazanavir (Reyataz; Bristol-Myers Squibb, New York, NY) were purchased from their respective sources. Drug tablets were pulverized with a pestle and mortar and dissolved in dimethyl sulfoxide (DMSO; Wako Pure Chemical Industries, Osaka, Japan). The concentration of each drug in DMSO was adjusted to 100 µg/ml with RPMI 1640 medium. To simulate the conditions of the drugs in the blood, the drug solutions were diluted 10-fold with normal plasma from Rhesus macaque. The drug extract was subsequently deproteinized by mixing with methanol/acetonitrile (1:1). The soluble fraction was evaporated, subsequently reconstituted in RPMI 1640 medium, and adjusted to a concentration of 20 µg/ml. Plasma samples collected from the animals were deproteinized, evaporated, and reconstituted as described above. The efficacy of the extraction employed in the current study ranged from 30-50% when assessed using the anti-HIV-1 drugs AZT, SQV, and RTV (data not shown).

Virus inhibition assay (MT-4/MTT assay)

The efficacies of the PIs against SIV were assessed as described previously (Sato et al., 1995), with minor modifications. Briefly, aliquots of 5×10^3 MT-4 cells were dispensed into 96-well round-bottomed tissue culture plates. Serially diluted extracts of the HIV-1 PIs or extracts of animal plasma samples were incubated with the cells in quadruplicate at 37°C for 1 h. The cells were then inoculated with 1.8×10^3 TCID₅₀ of SIV239 or 0.9×10^2 TCID₅₀ of HIV-1 IIIB (multiplicity of infection [MOI] = 0.37 or 0.018, respectively). On Day 5 pi, the viability of the cells was assessed by adding the MTT reagent (Nakalai Tesque).

Formulation and feeding of drugs and diet

The daily dosages of the drugs were half of those recommended for an adult human, i.e., 300 mg of AZT and 150 mg of 3TC (as Combivir; GlaxoSmithKline, London, UK), 150 mg of Tenofovir disoproxil fumarate (TDF, as Viread; Japan Tobacco, Tokyo, Japan), and 400 mg of Lopinavir and 100 mg of Ritonavir (as Kaletra; Abbott). To correlate these dosages for a 4-kg Rhesus macaque with the recommended dosage for an adult human, the body surface area (BSA) of the monkeys was computed as described previously (Du Bois and Du Bois, 1915; Du Bois and Du Bois, 1916). Using BSA and body weight, the *K_m* factor for each animal was derived as described (Reagan-Shaw et al., 2008). The dosage for the monkeys corresponded to 3-fold that for an adult human weighing 60 kg. Among the drugs selected, Combivir (AZT/3TC) and Kaletra (LPV/RTV) should be taken twice a day to maintain effective drug concentrations. Therefore, two sets of drug/diet were prepared. Formulation #1 contained AZT, 3TC, LPV, and RTV (150 mg, 75 mg, 200 mg, and 50 mg, respectively), while formulation #2 contained all the drugs in formulation #1 plus TDF (150 mg). Thirty-five grams of primate diet for Old World monkeys (Lab Diet 5048; PMI Nutrition International, Henderson, CO), granulated with a bar blender, were combined with the pulverized drugs. The drug/diet mixture was further mixed with 75 g of squashed banana and formed into a rectangular plate. The formulated drug/diet described above was given to animals in place of their normal diet. Drug/diet formulation #1 was given in the morning and formulation #2 was given 10 h later, at intervals of 10 h and 14 h per day. Seven of the nine Rhesus macaques that were fed the formulated drug/diet ingested 80-90% of total mass within 2 h.

To assess the potential adverse effects of the high-dosage drug administration employed in the current study, serum samples collected from these animals before and during cART were submitted to analyses for the following clinical markers: blood urea nitrogen (BUN), creatinine, total cholesterol, and triglycerides. No substantial fluctuations were observed before and during cART in the values for BUN (average values: for MM491, 16.8 mg/dl; for MM499, 16.0 mg/dl; for MM528, 16.7 mg/dl; and for MM530, 20.9 mg/dl), creatinine (average values: for MM491, 0.5 mg/dl; for MM499, 0.6 mg/dl; for MM528, 0.5 mg/dl; and for MM530, 0.5 mg/dl), and total cholesterol (average values: for MM491, 153 mg/dl; for MM499, 106 mg/dl; for MM528, 109 mg/dl; and for MM530, 132 mg/dl). Nearly all the samples analyzed fell within the normal value ranges for the above-mentioned markers (data not shown). The

triglyceride values from all the treated animals, with the exception of MM499, increased upon onset of ART: for MM491, the values ranged from 28 mg/dl at pretreatment to 99 mg/dl at maximum during cART; for MM528, from 21 mg/dl to 58 mg/dl; and for MM530, from 48 mg/dl to 129 mg/dl. The published normal value range for triglycerides in Rhesus macaques is 24–42 mg/dl (Fortman et al., 2001). At autopsy, lipid deposition in the liver was noted in MM530, which exhibited the highest mean level of triglycerides among the three animals, indicative of a certain degree of dysregulation of lipid metabolism. Despite the increase in triglyceride levels, all the treated animals were clinically healthy.

Lopinavir measurement by high-performance liquid chromatography

The drug concentrations in the blood samples were measured by high-performance liquid chromatography (HPLC) as described previously (Frappier et al., 1998), with minor modifications. Briefly, plasma samples collected from two monkeys were subjected to deproteinization by the addition of acetonitrile, and were subsequently loaded onto a HPLC column. The assay conditions were as follows: column, ODS column (150 mm in length and 4.6 mm in diameter; Cadenza); mobile phase, gradient prepared from two solutions (solution A, 0.1% trifluoroacetic acid [TFA] in water; solution B, 0.1% TFA in acetonitrile). The total flow rate was 0.6 ml/min. For detection of the compound, UV absorbance at a wavelength of 215 nm was employed.

Plasma viral RNA measurement

Viral RNA loads in plasma were measured as described previously (Miyake et al., 2006). Briefly, total RNA was extracted from plasma samples with the QIAamp Viral RNA kit (Qiagen, Valencia, CA). The extracted RNA samples were subjected to RT-PCR to amplify the SIV gag region using the TaqMan EZ RT-PCR kit (PerkinElmer, Wellesley, MA). The PCR and detection of products were performed in a Prism 7700 Sequence Detector (Applied Biosystems, Foster City, CA). The primer pair employed for PCR amplification was SIV2-696F (5'-GGAAATTACCCAGTACAACAAATAFF-3') and SIV2-784R (5'-TCTATCAATTTTACCCAggCATTTA-3'). PCR products were detected with a labeled probe, SIV2-731T (5'-Fam-TGTCCACCTGCCATTAAGCCCG-Tamra-3';

Perkin Elmer).

Selected plasma samples from monkeys on cART (at 29, 42, and 52 weeks pi, and at euthanasia) were further subjected to quantitative real-time PCR with a lower detection limit, following the method described by Cline *et al.*, with modifications (Cline et al., 2005). Briefly, 1.5-ml plasma samples were centrifuged at $20,000 \times g$ for 1 h to sediment virus particles. The pellets were incubated with a mixture of GuHCl (Sigma-Aldrich) and proteinase K (Invitrogen) for 60 min at 37°C and subsequently incubated with a mixture of GuSCN (Sigma-Aldrich) and glycogen (Roche Applied Science, Indianapolis, IN) for 5 min at room temperature, followed by precipitation with isopropanol. The precipitated RNA fractions were resuspended in water and subjected to RT-PCR, as described above. A standard curve of the reaction was constructed by plotting threshold cycles of serially diluted virus stocks containing known amounts of vRNA extracted in the same manner as the test plasma samples. The detection limit was defined by the standard curve with a correlation coefficient (> 0.96) constructed from a set of serial dilutions with reproducible amplification. The detection limit of the assay was consistently < 20 copies/ml.

Mathematical modeling and statistical analysis of decay rate

The decline in SIV239 RNA copies in the plasma during cART was evaluated using a mathematical model similar to that developed previously to quantify and analyze the decay of HIV-1 viremia in patients treated with combination anti-retroviral therapy (Perelson et al., 1997). Briefly, two distinct cellular compartments are assumed to contribute to the vRNA. The first compartment consists of CD4^{+} T cells (i.e., short-lived cells), T , which are infected with a constant, k , die with a rate constant, δ , and have a burst size of N . The second compartment consists of long-lived cells, M , which become infected with a rate constant, k_M , die with a rate, μ_M , and produce p virions per cell. Free virus particles are cleared with a constant, c . Assuming that viral inhibition by cART is 100%, *de novo* infection is completely blocked in this mathematical model. Then, using the parameters explained above, the overall vRNA

copies in the plasma can be described by the following equation:

$$V(t) = V_0 \left\{ \left(1 - \frac{NkT_0}{c - \delta} - \frac{c - NkT_0}{c - \mu_M} \right) e^{-ct} + \frac{NkT_0}{c - \delta} e^{-\delta t} + \frac{c - NkT_0}{c - \mu_M} e^{-\mu_M t} \right\}. \quad (1)$$

Here, V_0 and T_0 are the steady-state level of viral load and CD4⁺ T cells count before HAART, respectively. The derivation of equation (1) is explained in detail elsewhere (Perelson and Nelson, 1999). To fit the plasma viremia data with the two-compartment model, we estimated the parameters, δ , μ_M , and a composite parameter, NkT_0 , employing nonlinear least-squares regression (FindMinimum package of Mathematica ver. 7.0 software). Since virion clearance occurs too rapidly to estimate c from the available data in Rhesus macaques, we fixed $c = 62.1$ (determined previously) (Igarashi et al., 1999), although the change in c did not significantly change in our parameter estimates (data not shown). To derive the 68% confidence interval for each parameter, we employed a bootstrap method (Efron, 1979; Efron and Tibshirani, 1986) in which each experiment was simulated 1000 times. Statistical comparisons for continuously distributed variables between groups were performed with Welch's test. Nominal P -values <0.05 were considered statistically significant and all tests were two-sided.

Necropsy and tissue collection

All the animals were subjected to perfusion/euthanasia, as described previously (Igarashi et al., 2002), with minor modifications. Briefly, animals anesthetized with ketamine/xylazine were intravenously administered pentobarbital sodium (50 mg/kg body weight, Nembutal; Abbott Laboratories) before thoracotomy. The right atrium was incised and one liter of sterile saline anti-coagulated with heparin (5 U/ml) was introduced into the left ventricle *via* a 16G needle attached to infusion tubing. Peripheral blood was collected prior to perfusion. During the perfusion, tissue collection was conducted. Collected tissues were trimmed and placed into two independent workflows: submersion in RNAlater (Qiagen) and stored at -20°C until RNA extraction, and fixation in 4% paraformaldehyde in PBS at 4°C overnight, followed by embedding in paraffin wax for histopathologic analyses. The list of

collected tissues is summarized in Table 5.

Isolation, quantification, and statistical analysis of viral RNA from tissues

Tissues submerged in RNAlater and stored at -20°C were subjected to total RNA extraction using TRIzol reagent (Invitrogen) according to the manufacturer's recommendations. Briefly, 50–100 mg of each tissue resuspended in 1 ml of TRIzol reagent were homogenized with Lysing Matrix D (MP Biomedicals, Irvine, CA) using FastPrep FP120 (MP Biomedicals). Chloroform (0.2 ml) was added to the homogenate, and the aqueous phase was collected to a new tube after centrifugation at $12,000 \times g$ for 15 minutes at 4°C. The aqueous phase was mixed with 0.5 ml isopropanol, and the supernatant was removed after centrifugation at $12,000 \times g$ for 10 minutes at 4°C. Then, 1 ml of 75% ethanol was added to the pellet and, after centrifugation at $7,500 \times g$ for 5 minutes at 4°C, the supernatant was cleared. The total RNA sample was resuspended in RNase-free water and frozen at -80°C until use. The amount of RNA extracted from each tissue specimen was measured in a UV spectrophotometer (UV-1600; Shimadzu, Kyoto, Japan). Aliquots (1 µg) of RNA extracted from the various tissue samples were subjected to RT-PCR, to amplify the SIV gag region. The amounts of vRNA detected by PCR in a variety of tissues from treated animals and untreated controls, as described below, were compared using a Mann-Whitney test and GraphPad Prism software (GraphPad, La Jolla, CA).

Immunohistochemistry

Viral-protein-producing cells were visualized with an anti-SIV antibody and anti-CD35 antibody, as described previously (Inaba et al., 2009), with minor modifications. Briefly, tissue sections (4-µm thickness) were dewaxed with xylene, rehydrated through an alcohol gradient, submerged in Target Retrieval Solution (DAKO, Glostrup, Denmark), and processed in an autoclave for 10 min to unmask the antigens. Subsequently, the tissue sections were washed with Tris-buffered saline/Tween-20 (TBST), treated with REAL Peroxidase-Blocking Solution (DAKO) for 5 min, to deactivate endogenous peroxidase, and washed with TBST. The sections were incubated with an anti-SIV Nef mouse monoclonal antibody (diluted 1:500, clone 04-001; FIT Biotech, Tampere, Finland) at 4°C overnight. After washing with TBST, the sections were incubated at room temperature for 30 min with the Envision+ kit (a horseradish

peroxidase-labeled anti-mouse immunoglobulin polymer; DAKO), washed with TBST, visualized using diaminobenzidine (DAB) substrate (DAKO) as the chromogen, and rinsed in distilled water. Subsequently, the sections were treated at 95°C for 10 min with Target Retrieval Solution (DAKO), to deactivate the antibody added upstream in the procedure, washed with TBST, and incubated with the anti-CD35 mouse monoclonal antibody (diluted 1:50, clone Ber-MAC-DRC; DAKO) at 4°C overnight. After washing, the slides were incubated with Histofine Simple Stain AP (an alkaline phosphatase-labeled anti-mouse immunoglobulin polymer; Nichirei, Tokyo, Japan) at room temperature for 30 min, and washed with TBST. The specific antigen-antibody reaction was visualized with Blue Alkaline Phosphatase Substrate Kit III (Vector Laboratories, Burlingame, CA). The stained sections were examined under an Axiophot Universal microscope (Carl Zeiss, Oberkochen, Germany), and images were captured with the Nikon Digital Sight DS-Fi1 camera head and Nikon Digital Sight DS-L2 control unit (Nikon, Tokyo, Japan).

To identify the Nef-producing cells, slides of the tissue were stained with the anti-SIV antibody and anti-CD3 antibody. Sections were subjected to dewaxing and unmasking of antigens, as described above. Subsequently, the sections were incubated with the anti-SIV Nef mouse monoclonal antibody (diluted 1:500, clone 04-001; FIT Biotech) at 4°C overnight. After washing with TBST, the sections were incubated at room temperature for 30 min with anti-CD3 rabbit polyclonal antibody (diluted 1:50; DAKO), and washed with TBST. The sections were treated with Alexa Fluor 488 (diluted 1:200, fluorochrome-conjugated goat anti-mouse immunoglobulin G; Molecular Probes, Eugene, OR) and Alexa Fluor 594 (diluted 1:200; fluorochrome-conjugated goat anti-rabbit immunoglobulin G; Molecular Probes) for 1 hour, to visualize the bound anti-SIV Nef antibody and anti-CD3 antibody, respectively. The stained sections were examined using a Leica TCS SP2 AOBS confocal microscope (Leica Microsystems, Exton, PA) and the Leica image software (Leica Microsystems). Sections prepared from an SIV-infected monkey (MM521) and uninfected monkeys were stained in the same manner as those from cART and post-cART animals, as controls for the staining (Supplemental Figure 3).

ACKNOWLEDGEMENT

The authors are in debt to Drs. T. Sata and S. Nakamura for technical advice and critique on histochemical staining, Dr. A. Nomoto for continuous support, and member of the Igarashi laboratory for assistance of animal procedures and analyses. This work was supported by Research on HIV/AIDS [08062160 to T.I.] from the Ministry of Health, Labor and Welfare of Japan. S.I. was supported by JST PRESTO program.

REFERENCES

- Balzarini, J., Weeger, M., Camarasa, M. J., De Clercq, E., and Uberla, K., 1995. Sensitivity/resistance profile of a simian immunodeficiency virus containing the reverse transcriptase gene of human immunodeficiency virus type 1 (HIV-1) toward the HIV-1-specific non-nucleoside reverse transcriptase inhibitors. *Biochem Biophys Res Commun.* 211 (3), 850-6.
- Benlhassan-Chahour, K., Penit, C., Dioszeghy, V., Vasseur, F., Janvier, G., Riviere, Y., Dereuddre-Bosquet, N., Dormont, D., Le Grand, R., and Vaslin, B., 2003. Kinetics of lymphocyte proliferation during primary immune response in macaques infected with pathogenic simian immunodeficiency virus SIVmac251: preliminary report of the effect of early antiviral therapy. *J Virol.* 77 (23), 12479-93.
- Bourry, O., Mannioui, A., Sellier, P., Roucairol, C., Durand-Gasselin, L., Dereuddre-Bosquet, N., Benech, H., Roques, P., and Le Grand, R., 2010. Effect of a short-term HAART on SIV load in macaque tissues is dependent on time of initiation and antiviral diffusion. *Retrovirology.* 7, 78.
- Brenchley, J. M., Schacker, T. W., Ruff, L. E., Price, D. A., Taylor, J. H.,

- 1 Beilman, G. J., Nguyen, P. L., Khoruts, A., Larson, M., Haase, A. T.,
2 and Douek, D. C., 2004. CD4+ T cell depletion during all stages of HIV
3 disease occurs predominantly in the gastrointestinal tract. *J Exp Med.*
4 200 (6), 749-59.
- 5 Brennan, T. P., Woods, J. O., Sedaghat, A. R., Siliciano, J. D., Siliciano, R. F.,
6 and Wilke, C. O., 2009. Analysis of human immunodeficiency virus
7 type 1 viremia and provirus in resting CD4+ T cells reveals a novel
8 source of residual viremia in patients on antiretroviral therapy. *J Virol.*
9 83 (17), 8470-81.
- 10 Burton, G. F., Keele, B. F., Estes, J. D., Thacker, T. C., and Gartner, S., 2002.
11 Follicular dendritic cell contributions to HIV pathogenesis. *Semin*
12 *Immunol.* 14 (4), 275-84.
- 13 Buzon, M. J., Massanella, M., Llibre, J. M., Esteve, A., Dahl, V., Puertas, M.
14 C., Gatell, J. M., Domingo, P., Paredes, R., Sharkey, M., Palmer, S.,
15 Stevenson, M., Clotet, B., Blanco, J., and Martinez-Picado, J., 2010.
16 HIV-1 replication and immune dynamics are affected by raltegravir
17 intensification of HAART-suppressed subjects. *Nat Med.* 16 (4), 460-5.
- 18 Chun, T. W., Davey, R. T., Jr., Engel, D., Lane, H. C., and Fauci, A. S., 1999.
19 Re-emergence of HIV after stopping therapy. *Nature.* 401 (6756),
20 874-5.
- 21 Chun, T. W., Davey, R. T., Jr., Ostrowski, M., Shawn Justement, J., Engel, D.,
22 Mullins, J. I., and Fauci, A. S., 2000. Relationship between
23 pre-existing viral reservoirs and the re-emergence of plasma viremia
24 after discontinuation of highly active anti-retroviral therapy. *Nat Med.*
25 6 (7), 757-61.
- 26 Chun, T. W., Stuyver, L., Mizell, S. B., Ehler, L. A., Mican, J. A., Baseler, M.,
27 Lloyd, A. L., Nowak, M. A., and Fauci, A. S., 1997. Presence of an
28 inducible HIV-1 latent reservoir during highly active antiretroviral
29 therapy. *Proc Natl Acad Sci U S A.* 94 (24), 13193-7.
- 30 Cline, A. N., Bess, J. W., Piatak, M., Jr., and Lifson, J. D., 2005. Highly
31 sensitive SIV plasma viral load assay: practical considerations,
32 realistic performance expectations, and application to reverse
33 engineering of vaccines for AIDS. *J Med Primatol.* 34 (5-6), 303-12.

- 1 Connick, E., Mattila, T., Folkvord, J. M., Schlichtemeier, R., Meditz, A. L.,
2 Ray, M. G., McCarter, M. D., Mawhinney, S., Hage, A., White, C., and
3 Skinner, P. J., 2007. CTL fail to accumulate at sites of HIV-1
4 replication in lymphoid tissue. *J Immunol.* 178 (11), 6975-83.
- 5 Dinoso, J. B., Rabi, S. A., Blankson, J. N., Gama, L., Mankowski, J. L.,
6 Siliciano, R. F., Zink, M. C., and Clements, J. E., 2009. A simian
7 immunodeficiency virus-infected macaque model to study viral
8 reservoirs that persist during highly active antiretroviral therapy. *J*
9 *Virol.* 83 (18), 9247-57.
- 10 Douek, D. C., Picker, L. J., and Koup, R. A., 2003. T cell dynamics in HIV-1
11 infection. *Annu Rev Immunol.* 21, 265-304.
- 12 Du Bois, D., and Du Bois, E. F., 1915. The measurement of the surface area
13 of man. *Archives of Internal Medicine.* 15, 868-881.
- 14 Du Bois, D., and Du Bois, E. F., 1916. A formula to estimate the approximate
15 surface area if height and weight be known. *Archives of Internal*
16 *Medicine.* 17, 863-871.
- 17 Efron, B., 1979. 1977 Rietz Lecture - Bootstrap Methods - Another Look at
18 the Jackknife. *Annals of Statistics.* 7 (1), 1-26.
- 19 Efron, B., and Tibshirani, R., 1986. Bootstrap methods for standard errors,
20 confidence intervals, and other measures of statistical accuracy.
21 *Statistical Science* 1,54-75.
- 22 Embretson, J., Zupancic, M., Ribas, J. L., Burke, A., Racz, P., Tenner-Racz,
23 K., and Haase, A. T., 1993. Massive covert infection of helper T
24 lymphocytes and macrophages by HIV during the incubation period of
25 AIDS. *Nature.* 362 (6418), 359-62.
- 26 Finzi, D., Hermankova, M., Pierson, T., Carruth, L. M., Buck, C., Chaisson, R.
27 E., Quinn, T. C., Chadwick, K., Margolick, J., Brookmeyer, R., Gallant,
28 J., Markowitz, M., Ho, D. D., Richman, D. D., and Siliciano, R. F., 1997.
29 Identification of a reservoir for HIV-1 in patients on highly active
30 antiretroviral therapy. *Science.* 278 (5341), 1295-300.
- 31 Folkvord, J. M., Armon, C., and Connick, E., 2005. Lymphoid follicles are
32 sites of heightened human immunodeficiency virus type 1 (HIV-1)
33 replication and reduced antiretroviral effector mechanisms. *AIDS Res*

- 1 Hum Retroviruses. 21 (5), 363-70.
- 2 Fortman, J. D., Hewett, T. A., and Bennett, B. T., 2001. The Laboratory
- 3 Nonhuman Primate. CRC Press, New York.
- 4 Frappier, S., Breilh, D., Diarte, E., Ba, B., Ducint, D., Pellegrin, J. L., and
- 5 Saux, M. C., 1998. Simultaneous determination of ritonavir and
- 6 saquinavir, two human immunodeficiency virus protease inhibitors, in
- 7 human serum by high-performance liquid chromatography. J
- 8 Chromatogr B Biomed Sci Appl. 714 (2), 384-9.
- 9 Frost, S. D., Gunthard, H. F., Wong, J. K., Havlir, D., Richman, D. D., and
- 10 Leigh Brown, A. J., 2001. Evidence for positive selection driving the
- 11 evolution of HIV-1 env under potent antiviral therapy. Virology. 284
- 12 (2), 250-8.
- 13 Giuffre, A. C., Higgins, J., Buckheit, R. W., Jr., and North, T. W., 2003.
- 14 Susceptibilities of simian immunodeficiency virus to protease
- 15 inhibitors. Antimicrob Agents Chemother. 47 (5), 1756-9.
- 16 Guadalupe, M., Reay, E., Sankaran, S., Prindiville, T., Flamm, J., McNeil, A.,
- 17 and Dandekar, S., 2003. Severe CD4+ T-cell depletion in gut lymphoid
- 18 tissue during primary human immunodeficiency virus type 1 infection
- 19 and substantial delay in restoration following highly active
- 20 antiretroviral therapy. J Virol. 77 (21), 11708-17.
- 21 Harada, S., Koyanagi, Y., and Yamamoto, N., 1985. Infection of
- 22 HTLV-III/LAV in HTLV-I-carrying cells MT-2 and MT-4 and
- 23 application in a plaque assay. Science. 229 (4713), 563-6.
- 24 Havlir, D. V., Strain, M. C., Clerici, M., Ignacio, C., Trabattoni, D., Ferrante,
- 25 P., and Wong, J. K., 2003. Productive infection maintains a dynamic
- 26 steady state of residual viremia in human immunodeficiency virus
- 27 type 1-infected persons treated with suppressive antiretroviral
- 28 therapy for five years. J Virol. 77 (20), 11212-9.
- 29 Igarashi, T., Brown, C., Azadegan, A., Haigwood, N., Dimitrov, D., Martin, M.
- 30 A., and Shibata, R., 1999. Human immunodeficiency virus type 1
- 31 neutralizing antibodies accelerate clearance of cell-free virions from
- 32 blood plasma. Nat Med. 5 (2), 211-6.
- 33 Igarashi, T., Brown, C. R., Byrum, R. A., Nishimura, Y., Endo, Y., Plishka, R.

- 1 J., Buckler, C., Buckler-White, A., Miller, G., Hirsch, V. M., and Martin,
2 M. A., 2002. Rapid and irreversible CD4+ T-cell depletion induced by
3 the highly pathogenic simian/human immunodeficiency virus
4 SHIV(DH12R) is systemic and synchronous. *J Virol.* 76 (1), 379-91.
- 5 Inaba, K., Fukazawa, Y., Matsuda, K., Himeno, A., Matsuyama, M., Ibuki, K.,
6 Miura, Y., Koyanagi, Y., Nakajima, A., Blumberg, R. S., Takahashi, H.,
7 Hayami, M., Igarashi, T., and Miura, T., 2009. Small intestine CD4+
8 cell reduction and enteropathy in simian/human immunodeficiency
9 virus KS661-infected rhesus macaques in the presence of low viral
10 load. *J Gen Virol.* 91 (Pt 3), 773-81.
- 11 Keele, B. F., Tazi, L., Gartner, S., Liu, Y., Burgon, T. B., Estes, J. D., Thacker,
12 T. C., Crandall, K. A., McArthur, J. C., and Burton, G. F., 2008.
13 Characterization of the follicular dendritic cell reservoir of human
14 immunodeficiency virus type 1. *J Virol.* 82 (11), 5548-61.
- 15 Kestler, H., Kodama, T., Ringler, D., Marthas, M., Pedersen, N., Lackner, A.,
16 Regier, D., Sehgal, P., Daniel, M., King, N., and et al., 1990. Induction
17 of AIDS in rhesus monkeys by molecularly cloned simian
18 immunodeficiency virus. *Science.* 248 (4959), 1109-12.
- 19 Koyanagi, Y., Harada, S., and Yamamoto, N., 1986. Establishment of a high
20 production system for AIDS retroviruses with a human T-leukemic
21 cell line Molt-4. *Cancer Lett.* 30 (3), 299-310.
- 22 Markowitz, M., Louie, M., Hurley, A., Sun, E., Di Mascio, M., Perelson, A. S.,
23 and Ho, D. D., 2003. A novel antiviral intervention results in more
24 accurate assessment of human immunodeficiency virus type 1
25 replication dynamics and T-cell decay in vivo. *J Virol.* 77 (8), 5037-8.
- 26 Martinez, M. A., Cabana, M., Ibanez, A., Clotet, B., Arno, A., and Ruiz, L.,
27 1999. Human immunodeficiency virus type 1 genetic evolution in
28 patients with prolonged suppression of plasma viremia. *Virology.* 256
29 (2), 180-7.
- 30 Meng, G., Sellers, M. T., Mosteller-Barnum, M., Rogers, T. S., Shaw, G. M.,
31 and Smith, P. D., 2000. Lamina propria lymphocytes, not macrophages,
32 express CCR5 and CXCR4 and are the likely target cell for human
33 immunodeficiency virus type 1 in the intestinal mucosa. *J Infect Dis.*

- 1 182 (3), 785-91.
- 2 Miyake, A., Ibuki, K., Enose, Y., Suzuki, H., Horiuchi, R., Motohara, M.,
- 3 Saito, N., Nakasone, T., Honda, M., Watanabe, T., Miura, T., and
- 4 Hayami, M., 2006. Rapid dissemination of a pathogenic simian/human
- 5 immunodeficiency virus to systemic organs and active replication in
- 6 lymphoid tissues following intrarectal infection. *J Gen Virol.* 87 (Pt 5),
- 7 1311-20.
- 8 Murray, J. M., Emery, S., Kelleher, A. D., Law, M., Chen, J., Hazuda, D. J.,
- 9 Nguyen, B. Y., Teppler, H., and Cooper, D. A., 2007. Antiretroviral
- 10 therapy with the integrase inhibitor raltegravir alters decay kinetics
- 11 of HIV, significantly reducing the second phase. *AIDS.* 21 (17),
- 12 2315-21.
- 13 North, T. W., Higgins, J., Deere, J. D., Hayes, T. L., Villalobos, A., Adamson,
- 14 L., Shacklett, B. L., Schinazi, R. F., and Luciw, P. A., 2009. Viral
- 15 sanctuaries during highly active antiretroviral therapy in a
- 16 nonhuman primate model for AIDS. *J Virol.* 84 (6), 2913-22.
- 17 Palmer, S., Maldarelli, F., Wiegand, A., Bernstein, B., Hanna, G. J., Brun, S.
- 18 C., Kempf, D. J., Mellors, J. W., Coffin, J. M., and King, M. S., 2008.
- 19 Low-level viremia persists for at least 7 years in patients on
- 20 suppressive antiretroviral therapy. *Proc Natl Acad Sci U S A.* 105 (10),
- 21 3879-84.
- 22 Pantaleo, G., Graziosi, C., Demarest, J. F., Butini, L., Montroni, M., Fox, C.
- 23 H., Orenstein, J. M., Kotler, D. P., and Fauci, A. S., 1993. HIV infection
- 24 is active and progressive in lymphoid tissue during the clinically
- 25 latent stage of disease. *Nature.* 362 (6418), 355-8.
- 26 Pauwels, R., Balzarini, J., Baba, M., Snoeck, R., Schols, D., Herdewijn, P.,
- 27 Desmyter, J., and De Clercq, E., 1988. Rapid and automated
- 28 tetrazolium-based colorimetric assay for the detection of anti-HIV
- 29 compounds. *J Virol Methods.* 20 (4), 309-21.
- 30 Perelson, A. S., Essunger, P., Cao, Y., Vesanen, M., Hurley, A., Saksela, K.,
- 31 Markowitz, M., and Ho, D. D., 1997. Decay characteristics of
- 32 HIV-1-infected compartments during combination therapy. *Nature.*
- 33 387 (6629), 188-91.

- 1 Perelson, A. S., and Nelson, P. W., 1999. Mathematical analysis of HIV-1
2 dynamics in vivo. *Siam Review*. 41 (1), 3-44.
- 3 Popovic, M., Sarngadharan, M. G., Read, E., and Gallo, R. C., 1984.
4 Detection, isolation, and continuous production of cytopathic
5 retroviruses (HTLV-III) from patients with AIDS and pre-AIDS.
6 *Science*. 224 (4648), 497-500.
- 7 Reagan-Shaw, S., Nihal, M., and Ahmad, N., 2008. Dose translation from
8 animal to human studies revisited. *FASEB J*. 22 (3), 659-61.
- 9 Reed, L., and Muench, H., 1938. A simple method of estimating fifty percent
10 endpoints. *The american journal of hygiene*. 27, 493-497.
- 11 Richman, D. D., 2001. HIV chemotherapy. *Nature*. 410 (6831), 995-1001.
- 12 Sato, A., Kodama, M., Abe, K., Miki, S., Nishimura, M., Suyama, A., Ogata,
13 M., Toyoda, T., Sugimoto, H., Yoshie, O., and et al., 1995. A simple and
14 rapid method for preliminary evaluation of in vivo efficacy of anti-HIV
15 compounds in mice. *Antiviral Res*. 27 (1-2), 151-63.
- 16 Sharkey, M., Babic, D. Z., Greenough, T., Gulick, R., Kuritzkes, D. R., and
17 Stevenson, M., 2011. Episomal viral cDNAs identify a reservoir that
18 fuels viral rebound after treatment interruption and that contributes
19 to treatment failure. *PLoS Pathog*. 7 (2), e1001303.
- 20 Sharkey, M., Triques, K., Kuritzkes, D. R., and Stevenson, M., 2005. In vivo
21 evidence for instability of episomal human immunodeficiency virus
22 type 1 cDNA. *J Virol*. 79 (8), 5203-10.
- 23 Sharkey, M. E., Teo, I., Greenough, T., Sharova, N., Luzuriaga, K., Sullivan,
24 J. L., Bucy, R. P., Kostrikis, L. G., Haase, A., Veryard, C., Davaro, R. E.,
25 Cheeseman, S. H., Daly, J. S., Bova, C., Ellison, R. T., 3rd, Mady, B.,
26 Lai, K. K., Moyle, G., Nelson, M., Gazzard, B., Shaunak, S., and
27 Stevenson, M., 2000. Persistence of episomal HIV-1 infection
28 intermediates in patients on highly active anti-retroviral therapy. *Nat*
29 *Med*. 6 (1), 76-81.
- 30 Shibata, R., Kawamura, M., Sakai, H., Hayami, M., Ishimoto, A., and Adachi,
31 A., 1991. Generation of a chimeric human and simian
32 immunodeficiency virus infectious to monkey peripheral blood
33 mononuclear cells. *J Virol*. 65 (7), 3514-20.

- 1 Siliciano, J. D., Kajdas, J., Finzi, D., Quinn, T. C., Chadwick, K., Margolick, J.
2 B., Kovacs, C., Gange, S. J., and Siliciano, R. F., 2003. Long-term
3 follow-up studies confirm the stability of the latent reservoir for HIV-1
4 in resting CD4+ T cells. *Nat Med.* 9 (6), 727-8.
- 5 Spiegel, H., Herbst, H., Niedobitek, G., Foss, H. D., and Stein, H., 1992.
6 Follicular dendritic cells are a major reservoir for human
7 immunodeficiency virus type 1 in lymphoid tissues facilitating
8 infection of CD4+ T-helper cells. *Am J Pathol.* 140 (1), 15-22.
- 9 Thacker, T. C., Zhou, X., Estes, J. D., Jiang, Y., Keele, B. F., Elton, T. S., and
10 Burton, G. F., 2009. Follicular dendritic cells and human
11 immunodeficiency virus type 1 transcription in CD4+ T cells. *J Virol.*
12 83 (1), 150-8.
- 13 Van Rompay, K. K., Brignolo, L. L., Meyer, D. J., Jerome, C., Tarara, R.,
14 Spinner, A., Hamilton, M., Hirst, L. L., Bennett, D. R., Canfield, D. R.,
15 Dearman, T. G., Von Morgenland, W., Allen, P. C., Valverde, C.,
16 Castillo, A. B., Martin, R. B., Samii, V. F., Bendele, R., Desjardins, J.,
17 Marthas, M. L., Pedersen, N. C., and Bischofberger, N., 2004.
18 Biological effects of short-term or prolonged administration of
19 9-[2-(phosphonomethoxy)propyl]adenine (tenofovir) to newborn and
20 infant rhesus macaques. *Antimicrob Agents Chemother.* 48 (5),
21 1469-87.
- 22 Veazey, R. S., DeMaria, M., Chalifoux, L. V., Shvetz, D. E., Pauley, D. R.,
23 Knight, H. L., Rosenzweig, M., Johnson, R. P., Desrosiers, R. C., and
24 Lackner, A. A., 1998. Gastrointestinal tract as a major site of CD4+ T
25 cell depletion and viral replication in SIV infection. *Science.* 280
26 (5362), 427-31.
- 27 Veazey, R. S., Mansfield, K. G., Tham, I. C., Carville, A. C., Shvetz, D. E.,
28 Forand, A. E., and Lackner, A. A., 2000. Dynamics of CCR5 expression
29 by CD4(+) T cells in lymphoid tissues during simian
30 immunodeficiency virus infection. *J Virol.* 74 (23), 11001-7.
- 31 Witvrouw, M., Pannecouque, C., Switzer, W. M., Folks, T. M., De Clercq, E.,
32 and Heneine, W., 2004. Susceptibility of HIV-2, SIV and SHIV to
33 various anti-HIV-1 compounds: implications for treatment and

postexposure prophylaxis. *Antivir Ther.* 9 (1), 57-65.
Wong, J. K., Hezareh, M., Gunthard, H. F., Havlir, D. V., Ignacio, C. C., Spina, C. A., and Richman, D. D., 1997. Recovery of replication-competent HIV despite prolonged suppression of plasma viremia. *Science*. 278 (5341), 1291-5.

WEB REFERENCE

Department of Health and Human Services (DHHS) (2011). Guidelines for the use of antiretroviral agents in HIV-1-infected adults and adolescents. (<http://aidsinfo.nih.gov/contentfiles/AdultandAdolescentGL.pdf>)

FIGURE CAPTIONS

Figure 1. Effects of cART on plasma viral loads. Seven Rhesus macaques were inoculated with SIV239. Four animals, MM491, MM499, MM528, and MM530 (solid lines), were treated with cART (shaded areas). Animals MM510, MM496, and MM521 (dotted line) served as untreated controls. The detection limit of our RT-PCR assay is 200 RNA copies/ml, and samples with levels below the level of detection are plotted as 200 RNA copies/ml. †, time of euthanasia.

Figure 2. Nef-expressing cells detected in the iMLNs of animal MM511. (a) The section was stained with the anti-SIV Nef mouse monoclonal antibody. (b) Juxtaposition of Nef-expressing cells and CD35-positive FDCs in the follicle of an

iMLN from MM511. The sample was stained using the anti-SIV Nef mouse monoclonal antibody (brown) and the anti-CD35 mouse monoclonal antibody (blue). Original magnification, $\times 40$. The insets contain a higher-magnification, $\times 126$ equivalent (original magnification, $\times 63$).

Figure 3. Nef-positive T lymphocytes in the MLN of animal MM511. Tissue sections were stained using the anti-SIV Nef mouse monoclonal antibody (green, a and d) and the anti-CD3 rabbit polyclonal antibody (red, b and e). (c) Superimposed image of a and b. Nef-positive T cells are clustered in the follicles of the iMLN. (f) Superimposed image of d and e. The T cell is detected in the paracortical area of the sMLN. Original magnification, $\times 40$.

Supplemental Figure 1. Efficacies of commercially available anti-HIV-1 protease inhibitors against SIV239 and HIV-1 IIIB. The anti-SIV efficacies of Saquinavir (SQV), Lopinavir/Ritonavir (LPV/RTV), and Atazanavir (ATV) were evaluated in the MT-4/MTT assay. HIV-1 IIIB was used as a control virus. Each virus was inoculated to MT-4 cells in the presence of increasing amounts of extracts from the drug tablets in quadruplicate. Cell proliferation was assessed with the MTT reagent on Day 5 of infection.

Supplemental Figure 2. Decay of plasma viremia in four monkeys in group A that

received cART. Plasma viral loads were measured by quantitative RT-PCR. The theoretical decay curve (dashed bold line) was derived by nonlinear least-square fitting of the mathematical model of Equation 1 (described in *Materials and Methods*) to the plasma viral load. The dotted line represents the declination of virus particles produced by short-lived infected cells, $V_0 \frac{NkT_0}{c-\delta} e^{-\delta t}$, and the dot-dashed line expresses the decay of virions produced by long-lived infected cells, $V_0 \frac{c-NkT_0}{c-\mu_M} e^{-\mu_M t}$. The steady-state values of viral load, V_0 , are averages of measurements obtained at three time-points over 3 weeks prior to the onset of cART. The parameters δ , μ_M , and NkT_0 , were estimated simultaneously. The parameter estimates are as follows: MM491, $\delta = 0.495$, $\mu_M = 0.028$, and $NkT_0 = 61.90$; MM499, $\delta = 0.853$, $\mu_M = 0.089$, and $NkT_0 = 61.44$; MM528, $\delta = 0.707$, $\mu_M = 0.980$, and $NkT_0 = 61.68$; MM530, $\delta = 0.523$, $\mu_M = 0.053$, and $NkT_0 = 61.78$.

Supplemental Figure 3. Sections from the MLNs of untreated animal MM521 (a, b and c), and an uninfected animal (d, e and f), as positive and negative controls, respectively. The tissue sections were stained with the anti-SIV Nef mouse monoclonal antibody (green, a and d) and the anti-CD3 rabbit polyclonal antibody (red, b and e). (c) Superimposed image of a and b. Nef-positive T cells are observed in the follicles and the paracortical area of the MLN. (f) Superimposed image of d and e. T cells were not detected in the sMLN. Original magnification, $\times 40$.

Figure1
[Click here to download high resolution image](#)

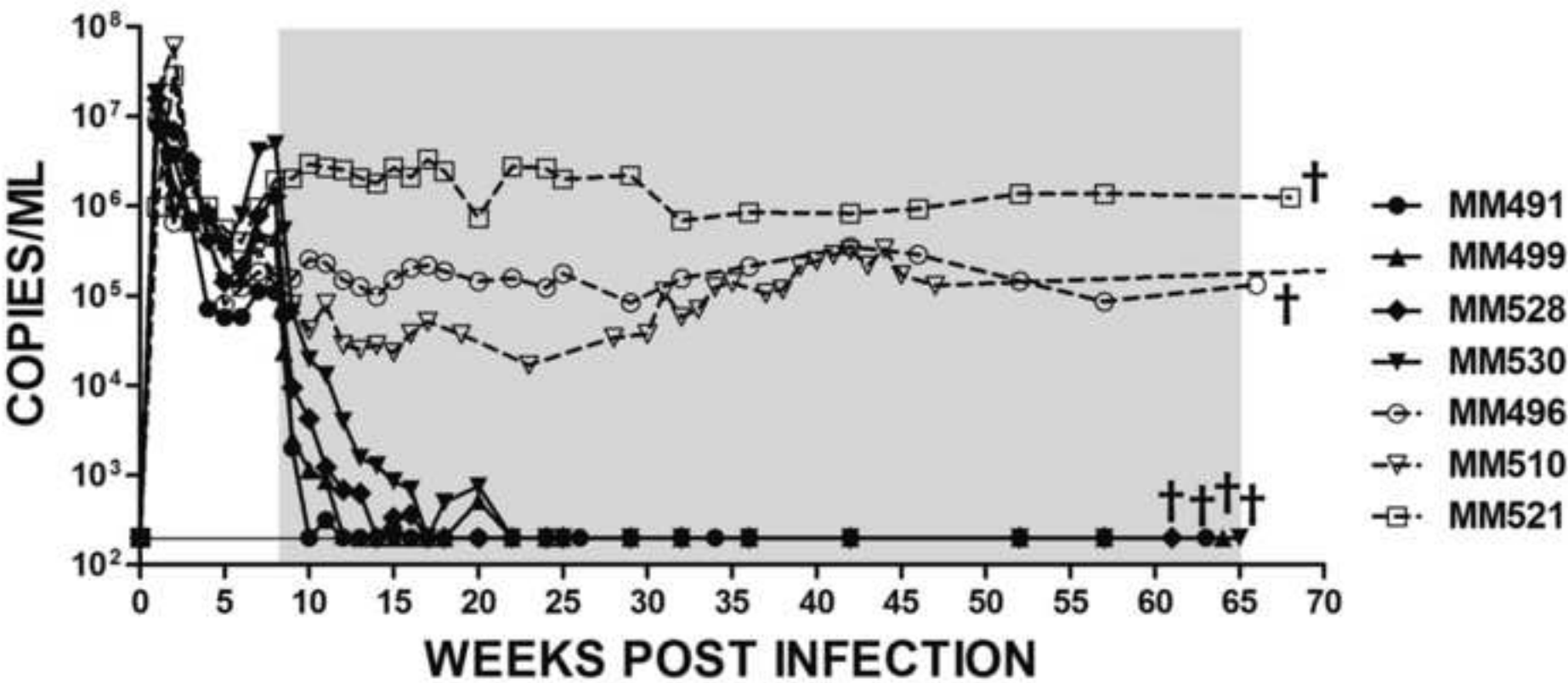


Figure2
[Click here to download high resolution image](#)

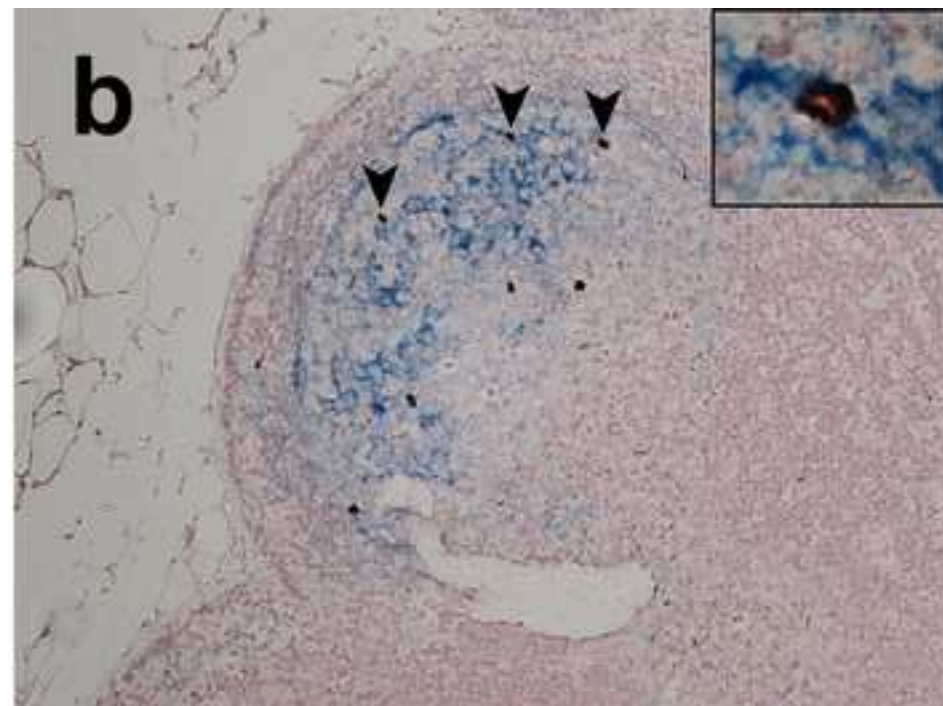
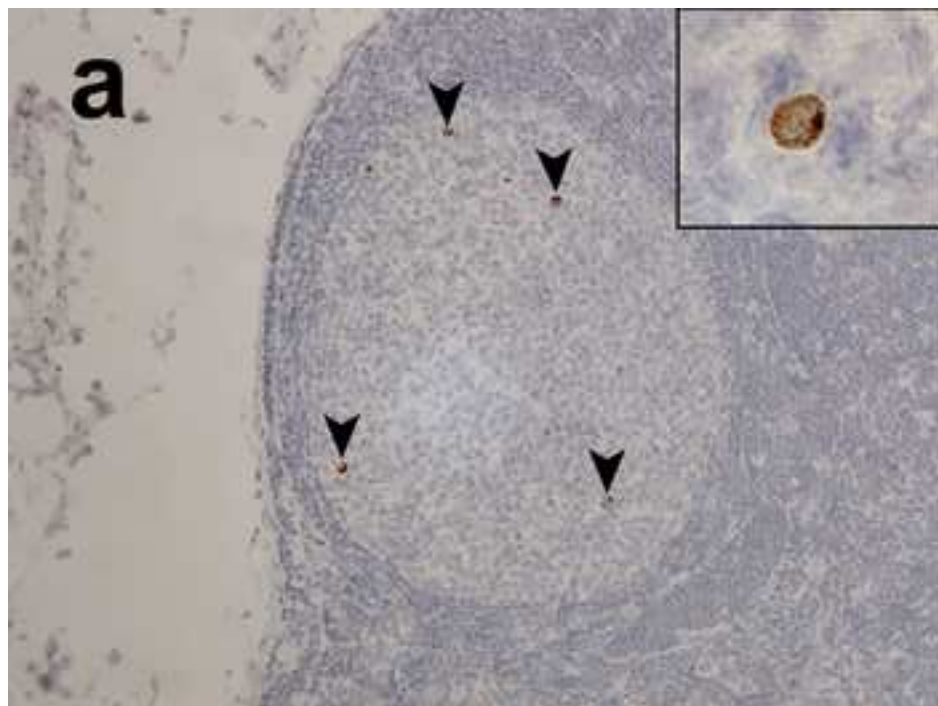


Figure3
[Click here to download high resolution image](#)

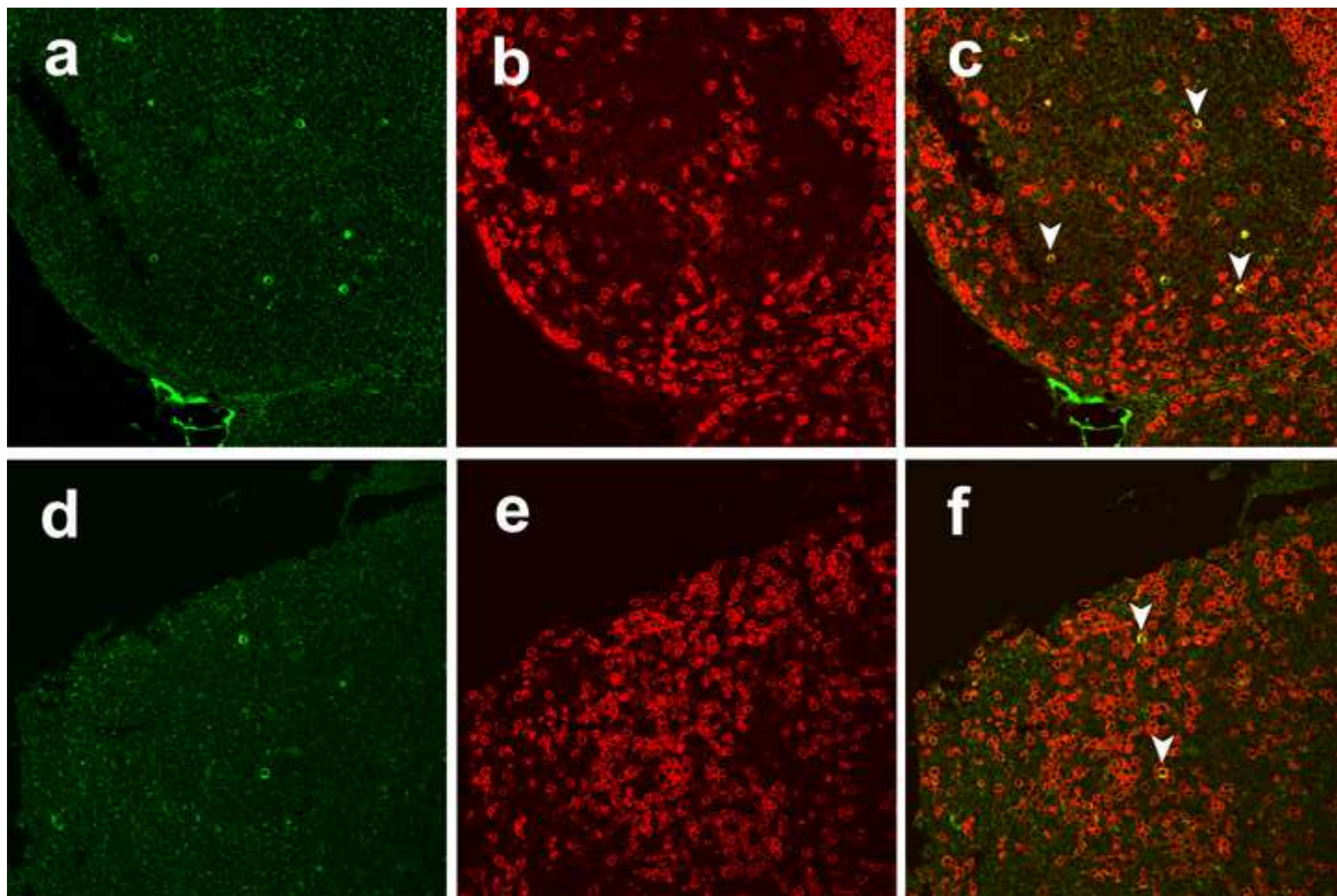


Table 1. Efficacies of commercially available anti-HIV-1 protease inhibitors against SIV239 and HIV-1 IIIB.

Compounds	EC ₅₀ ^a (nM)		EC ₅₀ ratio ^b
	SIV239	HIV-1 IIIB	
Saquinavir	18.5	22.7	0.8
Lopinavir/Ritonavir	52.2	35.6	1.5
Atazanavir	80.0	16.9	4.7

^a50 % effective concentration

^bEC₅₀ value against SIV239 divided by the EC₅₀ value against HIV-1 IIIB.

Table 2. Decay rate and half-life derived by mathematical modeling of short- or long-lived infected cells in group A monkeys.

Animal ID	Short-lived infected cells		Long-lived infected cells	
	Decay rate : a (day ⁻¹)	Half-life : $\log 2/a$ (days)	Decay rate : μ_M (day ⁻¹)	Half-life : $\log 2/\mu_M$ (days)
MM491	0.495 [0.405-0.605] ^a	1.400 [1.146-1.711]	0.028 [0.000-0.141]	24.76 [4.916- ∞]
MM499	0.853 [0.807-1.287]	0.813 [0.539-0.859]	0.089 [0.083-0.100]	7.753 [6.931-8.402]
MM528	0.707 [0.661-0.746]	0.980 [0.929-1.049]	0.061 [0.045-0.070]	11.44 [9.846-15.44]
MM530	0.523 [0.372-0.575]	1.325 [1.205-1.863]	0.053 [0.035-0.064]	13.00 [10.85-19.86]
Mean	0.645	1.130	0.058	14.24
S.D.	0.168	0.279	0.025	7.351

^aValues in parentheses represent the lower and upper 68% confidence intervals, calculated by a bootstrap method in which each experiment was simulated 1000 times.

Table 3. Plasma viral loads of selected samples measured by RT-PCR with a lower detection limit (20 copies/ml) in group A animals during cART.

Animals ID	Plasma viral loads (copies/ml)			
	29wpi	42wpi	52wpi	At autopsy ^a
MM491	< 20	< 20	< 20	< 20
MM499	< 20	< 20	< 20	< 20
MM528	< 20	< 20	< 20	< 20
MM530	< 20	44	47	< 20

^aMM491, 63 wpi; MM499, 64 wpi; MM528, 61 wpi; MM530, 65 wpi.

Table 4. Antiretroviral activities detected in the blood of animals in group A during cART.

Animals ID	Drug concentration (μM) ^a					At autopsy ^b
	10wpi	20wpi	32wpi	42wpi	56wpi	
MM491	3.5	15.9	12.1	17.8	7.9	5.2
MM499	0.6	2.3	4.4	11.4	1.7	0.9
MM528	16.0	24.9	6.6	7.7	6.0	9.3
MM530	9.4	12.4	8.2	14.2	11.3	11.3

^aLPV/RTV equivalent concentration.

^bMM491, 63 wpi; MM499, 64 wpi; MM528, 61 wpi; MM530, 65 wpi.

Table 5. Viral RNA burdens in various tissues collected from SIV-infected macaques.

Tissues	vRNA levels (copies/ µg total RNA)				
	treated with cART				untreated
	MM491	MM499	MM528	MM530	MM521
	<200 copies/ml ^a	<200 copies/ml ^a	<200 copies/ml ^a	<200 copies/ml ^a	1.2×10 ⁶ copies/ml ^a
Non-lymphoid tissues					
heart	<2900	<2900	<2900	<2900	3.0×10 ³
liver	<2900	<2900	<2900	<2900	8.8×10 ⁴
kidney	<2900	<2900	<2900	<2900	2.1×10 ⁶
CNS tissues					
cerebrum	<2900	<2900	<2900	<2900	1.1×10 ⁶
cerebellum	<2900	<2900	<2900	<2900	4.5×10 ³
brain stem	<2900	<2900	<2900	<2900	<2900
Effector sites					
lung	4.7×10 ³	4.1×10 ³	<2900	<2900	1.0×10 ⁵
vagina	6.5×10 ³	<2900	<2900	2.9×10 ³	1.3×10 ⁵
jejunum	5.0×10 ³	3.1×10 ³	1.1×10 ⁴	7.4×10 ³	1.7×10 ⁶
ileum	5.2×10 ³	4.0×10 ³	7.7×10 ³	<2900	1.4×10 ⁶
colon	1.8×10 ⁴	<2900	6.5×10 ⁴	8.3×10 ³	2.0×10 ⁸
rectum	2.9×10 ³	<2900	6.0×10 ³	9.9×10 ³	4.7×10 ⁶
Lymphoid tissues					
spleen	2.6×10 ⁴	5.0×10 ³	5.4×10 ³	6.2×10 ³	3.4×10 ⁸
thymus	<2900	<2900	N.D.	2.0×10 ⁵	2.9×10 ⁴
iliac LN	5.8×10 ⁴	6.9×10 ³	1.5×10 ⁴	3.6×10 ⁴	1.6×10 ⁸
inguinal LN	<2900	2.4×10 ⁴	2.4×10 ⁴	2.3×10 ⁵	6.9×10 ⁷
axillary LN	8.6×10 ⁴	7.2×10 ³	3.1×10 ⁴	2.1×10 ⁵	7.6×10 ⁷
iMLN	1.0×10 ⁵	8.8×10 ⁴	<2900	2.9×10 ⁵	1.0×10 ⁸
sMLN	1.3×10 ⁵	5.7×10 ⁴	3.4×10 ⁴	2.4×10 ⁵	2.3×10 ⁸
submandibular LN	6.2×10 ⁴	2.9×10 ⁴	1.6×10 ⁴	5.6×10 ³	3.9×10 ⁷
bronchial LN	1.5×10 ⁵	5.3×10 ⁴	3.1×10 ⁴	3.8×10 ⁵	1.1×10 ⁸
splenic LN	2.5×10 ⁵	4.3×10 ⁴	7.3×10 ³	2.0×10 ⁵	9.8×10 ⁷

N.D., no data; CNS, central nervous system; LNs, lymph nodes; iMLNs, inferior mesenteric lymph nodes; sMLNs, superior mesenteric lymph nodes.

Viral RNA levels (copies/µg total RNA) are coded in grayscale as follows: white boxes, <2900; light-gray boxes, <1.0×10⁵; dark-gray boxes, <1.0×10⁷; black boxes, >1.0×10⁷.

^aViral loads in plasma.

Table 6. Viral loads in plasma samples of animals in group B.

Animal ID	plasma viral loads (copies/ml)					
	0wpi	2wpi	8wpi	38wpi	46wpi	At autopsy ^a
MM508	<200	8.4×10^6	2.6×10^5	3.8×10^4	<200	<200
MM511	<200	7.7×10^6	3.1×10^5	1.1×10^5	<200	1.4×10^3

The animals were treated with cART from 38 wpi to 46 wpi.

^a47.5 wpi

Table 7. Viral RNA burdens in various tissues collected from animals in group B.

Tissues	vRNA levels (copies/ μ g total RNA)	
	MM508	MM511
	PVL, <200 copies/ml	PVL, 1400 copies/ml
Non-lymphoid tissues		
heart	<2900	<2900
liver	<2900	<2900
kidney	<2900	<2900
CNS tissues		
cerebrum	<2900	<2900
cerebellum	<2900	<2900
brain stem	<2900	<2900
Effector sites		
lung	<2900	<2900
vagina	<2900	N.D.
upper intestinal tract	<2900	<2900
lower intestinal tract	<2900	<2900
Lymphoid tissues		
spleen	2.0×10^5	7.4×10^5
thymus	<2900	<2900
iliac LN	1.4×10^4	3.5×10^5
inguinal LN	<2900	5.3×10^5
axillary LN	1.9×10^4	1.3×10^6
iMLN	1.3×10^5	1.6×10^6
sMLN	8.4×10^3	1.5×10^6
submandibular LN	1.1×10^5	9.4×10^5
bronchial LN	1.1×10^4	9.5×10^5
splenic LN	9.9×10^4	N.D.

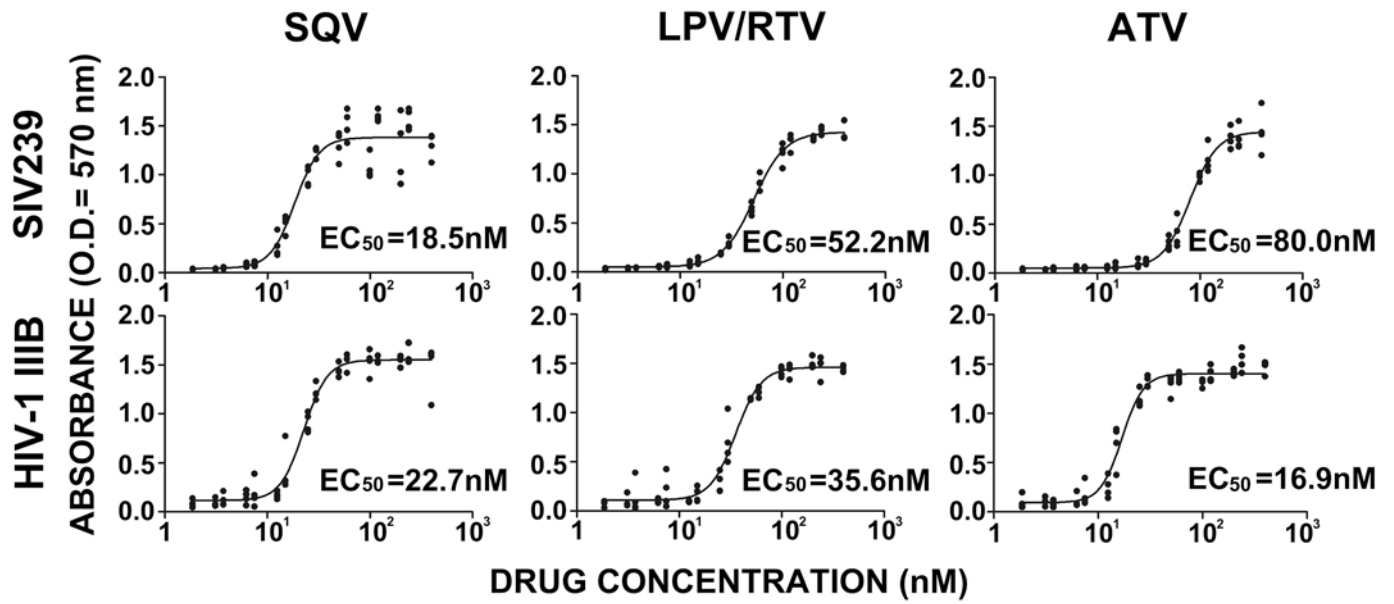
PVL, plasma virus load; N.D., no data; CNS, central nervous system; LNs, lymph nodes; iMLNs, inferior mesenteric lymph nodes; sMLNs, superior mesenteric lymph nodes.

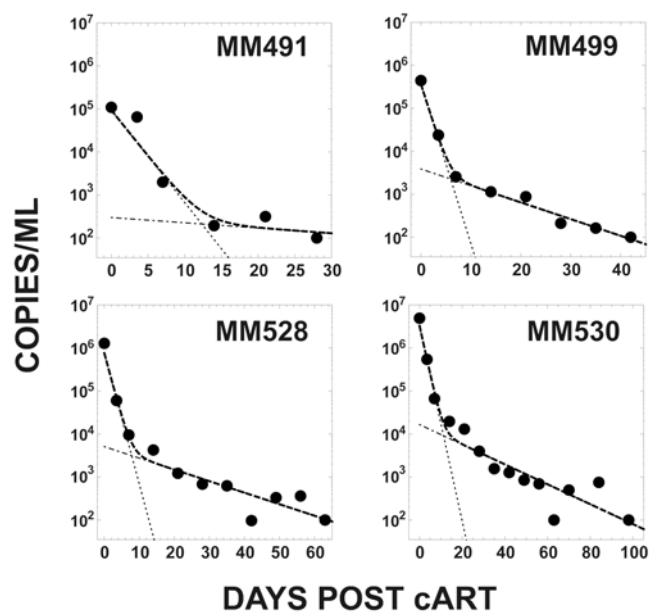
Viral RNA levels (copies/ μ g total RNA) are colored in grayscale as follows: white boxes, <2900; light-gray boxes, $<1.0 \times 10^5$; dark-gray boxes, $<1.0 \times 10^7$.

Table 8. Numbers of immunohistochemistry sections examined from macaques in group B.

Nef expressing T cells	Number of sections subjected				total
	MM508		MM511		
	MLN	Non-MLN	MLN	Non-MLN	
present in the follicles	0	0	9	3	12
present in the paracortical area	1	0	3	1	5
absent	50	85	34	255	424

MLNs; mesenteric lymph nodes.





Supplementary Figure 3.

